Journal of Hazardous Materials, 30 (1992) 117–150
Elsevier Science Publishers B.V., Amsterdam

Dispersion of a dense cylindrical cloud in a turbulent atmosphere

C.S. Matthias

Atmospheric Environment Service, 4905 Dufferin Street, Downsview, Ontario M3H 5T4 (Canada)

(Received February 4, 1991; accepted July 6, 1991)

Abstract

This paper describes the development of a simple analytical dense gas model. It calculates the height, radius, and instantaneous concentration within a drifting cloud. The initial state is a cylinder of gas of arbitrary aspect ratio. Upon release, the cylinder collapses due to its excess density. The collapse generates internal turbulence which entrains air and dilutes the cloud. Within the core or central part of the cloud, top entrainment controls concentration decay. The core concentration decays as t^{-1} (where t denotes time). Side entrainment generates a radial transition zone between the radially uniform core and the atmosphere. The core radius increases due to gravitational slumping and is eroded by side entrainment. Both the vertical and radial transition zones are chosen to be Gaussian. As the gravitational collapse continues, self-generated turbulence grows weaker. Internal turbulence, and hence entrainment, then becomes proportional to the ambient atmospheric turbulence divided by the Richardson number Ri where Ri is large and decreasing. This causes a vertical growth proportional to t^2 of the relatively thin disk. Gravitational slumping continues to maintain the radial growth such that $R^2 \sim t$ (R is the mean radius of cloud). Hence, concentration decays as t^{-3}. As Ri falls below the critical value Ri_c, the core vanishes and there is a smooth and gradual transition to a Gaussian puff description of the cloud. The non-dimensional concentration is shown to be primarily a function of non-dimensional time and a characteristic Richardson number. In addition to predicting the concentration field, the model calculates the cloud position as it accelerates from rest due to momentum entrainment from the ambient wind. Four data sets are used to calibrate and evaluate the model. The data are derived from laboratory studies at the University of Arkansas and at Colorado State University and from field studies at Porton Down and Thorney Island. The initial volumes of the gas clouds span eight orders of magnitude. Uncertainty of physical measurements and model estimates is discussed in detail. A mechanism for comparing modelled and measured concentrations (the ratio method) is used to quantify the uncertainty in a concentration estimate. Components of uncertainty are examined (inherent, model, observational, and input).

1. Introduction

This paper describes the development of a model to predict the height, radius, concentration, and downwind location of a drifting dense gas cloud. Its

Correspondence to: Dr. C.S. Matthias, Atmospheric Environment Service, 4905 Dufferin Street, Downsview, Ontario M3H5T4, Canada.

initial shape is cylindrical, defined by a height H, and diameter D (or radius R). The cloud drifts over a flat surface of uniform roughness, and accelerates from rest within a stationary wind field having a neutral logarithmic profile in the vertical direction. The time scale within which the model has been evaluated is 1000τ (τ is a characteristic time which is defined later). The use of a cylindrical model has several advantages: (1) It is mathematically tractable, (2) Several experiments with cylindrical symmetry have produced extensive data, (3) Most explosive or rapid releases will tend toward cylindrical symmetry as they evolve in a windless environment. Although a wind will distort a cylindrical shape in reality, it is still a useful model to investigate.

Dense gas models are important components of emergency response systems as well as important tools for environmental impact assessments and risk assessments. Dense gases have dispersion properties which are significantly different from neutral and buoyant gases.

The model begins as a uniform cylinder of dense gas. Pulled downward by gravity, it collapses, entrains air, becomes dilute, grows in volume, and maintains circular symmetry. It also entrains momentum which is the mechanism for accelerating the cloud towards the local wind speed. We assume that during the initial collapse, a fraction of the initial potential energy is immediately converted to cloud turbulence. Entrainment is proportional to this turbulence which decays monotonically. Both top and side entrainment are important. Because the cloud aspect ratio (H/D) rapidly becomes small, top entrainment forms a smooth concentration distribution ranging from a maximum at the surface to zero above the cloud. The distribution is assumed to be Gaussian.

Similarly, side entrainment causes radial erosion into the cylinder and also establishes a Gaussian transition zone. At the same time, the cylinder radius grows rapidly due to kinematic spreading as the cylinder slumps. The net effect is to maintain a core of radially invariant concentration whose radius R_c depends on the relative magnitudes of the kinematic and erosion growth rates. In general, the core has a net growth until the Richardson number Ri becomes small enough to allow atmospheric turbulence to control the entrainment process. While the core exists, its concentration is a function of top entrainment and kinematic spreading. When its vanishes, the maximum concentration is a function of top and side entrainment alone as the cloud makes a smooth transition to a Gaussian puff. However, the characteristic dimensions (σ_x, σ_y, σ_z) of the puff continue to retain the memory of the kinematic spreading for a long time.

More detail on the cloud growth during gravitational settling is given in Matthias [1]. The paper examines the properties of a dense gas cloud as it spreads and diffuses within an atmosphere having no wind or ambient turbulence. In a calm environment, the cloud differentiates into a central disk surrounded by a torus. The torus is transitory in nature and is eventually reabsorbed into the disk. The central disk is modelled as having a core consisting

of a radially invariant concentration field. Surrounding the core is a Gaussian fringe within which the gas concentration falls to zero. The temporal decay of the disk concentration is slow relative to that of the torus. In the interest of having a simple model which can describe the major properties of a dense gas cloud, the torus is ignored in the present paper. The present cloud is described by the equations for the central disk alone [1].

Since the equations in [1] are for a calm atmosphere, they must be modified to encompass both wind and turbulence in order to be more generally applicable. There is a large number of such models already available in the literature. Perhaps the most extensive review was done in 1984 by Wheatley and Webber [2]. It examines in detail some 45 dense gas models which range from analytical to 3-dimensional finite-difference codes. Of primary interest to the present paper are the simple analytical box models for instantaneous releases. These models have the capability of containing enough physics for describing the major features of dense gas dispersion such as mean temperature, density, concentration, height, and radius, However, because there is such a variety of ways for parameterizing entrainment, there are enormous differences in the various model solutions.

Britter [3] finds that practically no adequate model validation has been applied to the 100 or so dense gas models that have arisen in the past decade. Furthermore, the criteria for model evaluation are not standardized. The acceptability of an air quality model has often been determined by a visual assessment of the model curve passing through a few data points or by a comparison with other model results.

The present paper is concerned with addressing the problem of entrainment into a finite cloud which begins as a cylinder. In order to eliminate conflicting processes, we will examine only isothermal releases. The review by Wheatley and Webber [2] also examines entrainment expressions and experiments as does a review by Britter [4]. There is no consensus as to which of a variety of expressions is the best. The present model uses the gravitationally induced initial entrainment mechanism as explained in [1]. Most entrainment expressions assume that when the initial gravitationally induced entrainment becomes negligible, the entrainment velocity, v_e, due to atmospheric turbulence can be expressed as

$$v_e \propto q/Ri^{\mu} \tag{1}$$

where q is a measure of the turbulent velocity, Ri is a turbulent Richardson number, and μ is a constant of order unity [2], [4]. The concentration models, properly nondimensionalized, show concentration to be a function of time with the initial value of Ri (Ri_0) as a parameter.

It is unproductive to attempt to review here the variety of the various dense gas dispersion models. This is adequately done in the above-mentioned references. Three tables by Webber [5] show vividly the differences of opinion,

degree of complexity, and deviation of solutions. We propose to use simple box model physics to describe the evolution of properties such as maximum concentration, mean radius, and mean height. These will be considered to be acceptable if there is reasonable correlation of model and data results between several parameters using several data sources.

The key problems in dense gas dispersion modelling of an inert gas in isothermal conditions in the atmosphere seem to be (1) choosing an appropriate entrainment mechanism, and (2) making a smooth transition from a cylindrical slab model to a Gaussian-type puff model. The former is the more difficult problem and deals with the relative importance of top and side entrainment and with the details of the entrainment processes themselves. Turner [6] provides a convenient interpretation as well as a simple expression for vertical entrainment into a stable fluid of height H and density ρ. His expression which links all the relevant variables is

$$g(\rho-\rho_a)Hv_e \propto \rho_a u_*^3 \tag{2}$$

where g is the gravitational constant, ρ_a is the density of air, and u_* is the ambient friction velocity. His interpretation of eq. (2) is that the rate of increase of potential energy of the stable layer is proportional to the rate of work done by the surface stress. Equation (2) can be written as

$$v_e/u_* \propto Ri_*^{-1} \tag{3}$$

where the bulk Richardson number is written as

$$Ri_* = (\rho-\rho_a)gH/\rho_a u_*^2 \tag{4}$$

Following the development of an entrainment model based upon eq. (3), the smooth transition of a stably stratified cloud to a neutrally stratified cloud is examined. Then a mechanism for evaluating the model is described and model results are compared to data. There are several sources of uncertainty, each of which is discussed.

2. Equation for gravity front velocity

The equation for the frontal speed of a gravity current is usually given as

$$U_f = a_1(gH\Delta)^{1/2} \tag{5a}$$

or

$$U_f = a_1(gH\Delta')^{1/2} \tag{5b}$$

or

$$U_f = a_1(gH\Delta'')^{1/2} \tag{5c}$$

where $\Delta = (\rho-\rho_a)/\rho_a$, $\Delta' = (\rho-\rho_a)/\rho$, and $\Delta'' = (\rho-\rho_a)/\rho'$. The density ρ' is

of indefinite size but is representative of the problem (i.e., $\rho_a \leq \rho' \leq \rho$). As long as the densities, ρ, ρ_a, ρ' are similar, eqs. (5) are equivalent. The constant a_1 is of order 1 and can be determined by experiment. The equation for U_f is central to the description of cloud kinematic and dispersive growth and yet its origin seems to be obscure. The equations have been shown experimentally to be a very good measure of radial growth. Perhaps because of this, eqns. (5) are presented almost axiomatically in most papers of dense gas dispersion. Equation (5a) can be derived by balancing a pressure head against a form drag [2]. Equation (5b) is derived from conservation of mass, momentum, and energy [6]. An order of magnitude analysis by Fay [7] in which gravity and inertia forces are balanced yields eq. (5c).

It is common for the gas density to exceed the air density by a factor of four in controlled experiments with freon 12. The density ratio could be much higher with other gases. For large density differences, the frontal speed of eq. (5a) exceeds that of eq. (5b) by a factor $(\rho/\rho_a)^{1/2} = (MT_a/M_aT)^{1/2}$, neglecting aerosol contributions to the density. M, T and M_a, T_a are the molecular weight and temperature of the gas mixture and ambient air, respectively. For reasons which are usually unspecified, eq. (5a) is more frequently used. However, Byggstoyl and Saetran [8] note that eq. (5a) is physically incorrect, since it allows a cloud to have a larger kinetic energy than its initial potential energy. Pursuing this further, the maximum possible velocity can be estimated by equating the cloud kinetic energy to the initial potential energy, i.e.,

$$\rho U_f^2/2 \approx (\rho - \rho_a) g H_0/2 \tag{6}$$

where H_0 is the initial height of the cloud. Furthermore, eq. (5b) can be derived quite simply by applying Bernoulli's equation along a radius at the bottom of the cloud.

If eq. (5b) is the correct equation for the speed of a gravity front, why is it not used more frequently and with greater success? Let us rewrite eqs. (5a) and (5b) in terms of the buoyancy b:

$$\frac{dR}{dt} = U_f = a_1 b^{1/2}/R \tag{7a}$$

and

$$\frac{dR}{dt} = U_f = a_1 b'^{1/2}/R \tag{7b}$$

where $b = gV\Delta/\rho$, $b' = gV\Delta'/\pi$, and cloud volume $V = \rho R^2 H$. If there is no entrainment, V, Δ, Δ', b, and b' all remain constant at their initial values V_0, Δ_0, Δ_0', b_0, and b_0' respectively, and $b > b'$. If there is entrainment, V grows as Δ and Δ' decrease. Fortuitously, b remains constant ($b = b_0$) for a wide class of flows which are (i) isothermal or (ii) nonisothermal in which the gas and air

molar specific heats are equal and for which ground heating is negligible [2]. This allows eq. (7a) to be easily integrated and accounts for its popularity.

Similarly, if b' can be shown to be constant, eq. (7b) can be analytically integrated and used with confidence with $b' = b'_0$. Following the analysis of Wheatley and Webber [2], the expression for b' can be shown to be

$$b' = \frac{b_0}{\frac{T_a}{T} + \frac{m_g}{\rho_a V}\left(1 - \frac{M_a}{M_g}\right)} \tag{8}$$

where m_g and M_g are the mass and molecular weight, respectively, of contaminant gas. Hence, b' will be constant only under the exceptional circumstances of no entrainment and no heat transfer. In general, there is entrainment during which T and V vary, precluding a simple integrated form for eqn. (7b). However, as time progresses, $T \to T_a$ and $V \gg V_0$. The limiting values of b' are then

$$b'_0 = \frac{T_0 M_a}{T_a M_g} b_0 \qquad t = 0 \tag{9}$$

and

$$b'_\infty = b_0 \qquad t \to \infty \tag{10}$$

Most experimental dense cloud releases have had aspect ratios of order 1. The entrainment has been vigorous enough such that $V \geqslant 10 V_0$ when $t \geqslant 50\tau$ [1]. This means that $b' \to b_0$ early in the life of the cloud and remains equal to b_0 as long as the radial growth is controlled by gravitational spreading (i.e., $Ri > Ri_c$). Hence, eqns. (7) are practically identical during most of the gravity flow period and have the same simple analytical solution. They differ only for small times t during which neither equation is accurate since radial acceleration of the expanding cloud from a state of rest is ignored.

The characteristic time τ is a measure of the time required for the accelerating density front to achieve its maximum speed. It is an important scaling parameter and is responsible for collapsing concentration vs. time data along a single curve. The expression for τ is given by

$$\tau = (l/g\Delta_0)^{1/2} \tag{11}$$

where Δ_0 is the initial value of Δ and $l = V_0^{1/3}$ is a characteristic scaling length [1].

3. Entrainment and cloud growth

When the cylindrical cloud is released at $t = 0$, there are several entrainment mechanisms in operation. Initially, the dominant entrainment is due to internal turbulence created by the sudden collapse of the cylinder. At the same time,

external ambient turbulence is attempting to penetrate the relatively stable dense cloud and gradually becomes more successful as the cloud Richardson number decreases. Also, molecular diffusion is continually acting to weaken any density gradients. The latter becomes important only for small volume releases in the laboratory where the cloud height is small.

The equations of the following Sections 3.1 and 3.2 are taken from Matthias [1] where their origins are explained in detail. They are repeated here only to assist in adapting them to the new material of Section 3.3.

3.1 The concentration equations

Gradually and smoothly, the cylinder is transformed into a Gaussian puff ellipsoid. Concomitantly, the coordinate system changes smoothly from a cylindrical r,z system to a Cartesian x,y,z system. The wind blows along the x-axis. The primary concentration predicted by the model is the maximum concentration which is located at the centreline surface. It begins as a bulk value C_b from a bulk or box cylindrical model. The spatial distribution of concentrations about the maximum is described by Gaussian relations as

$$C = C_b \exp(-z^2/2\sigma_z^2) \qquad r < R_c \tag{12a}$$

$$= C_b \exp(-z^2/2\sigma_z^2) \exp[-(r-R_c)^2/2\sigma_r^2] \qquad r > R_c \tag{12b}$$

where

$$C_b = \frac{m_g}{\pi R^2 H} \qquad \text{while } R_c > 0 \tag{13a}$$

$$= \frac{2m_g}{(2\pi)^{3/2}\sigma_r^2\sigma_z} \qquad \text{later, when } R_c = 0 \tag{13b}$$

The core radius R_c is given by the following quadratic equation [1]:

$$R^2 = R_c^2 + (2\pi)^{1/2} R_c \sigma_r + 2\sigma_r^2 \tag{14}$$

The characteristic radial and vertical dimensions (sigmas σ_r and σ_z) of the Gaussian distributions describe the growth of the cloud due to turbulent and molecular random processes. The source of the turbulence is (1) the violence and shear of the initial cloud collapse and (2) the ambient atmosphere. Since the dispersive sources are independent of one another, the net magnitude of the sigmas can be expressed as

$$\sigma_r^2 = \sigma_{rg}^2 + \sigma_{ra}^2 \tag{15}$$

$$\sigma_z^2 = \sigma_{zg}^2 + \sigma_{za}^2 + \sigma_m^2 \tag{16}$$

where the subscripts 'g' and 'a' refer to gravitational collapse and ambient atmospheric turbulence, respectively. The contribution due to molecular diffusion σ_m is not included in σ_r since it is always much smaller than the gravi-

tational component σ_{rg} initially and the atmospheric component σ_{ra} later. The component sigmas on the right hand sides above will be explained in the following sections. The cloud height H is related to σ_z by

$$H=(\pi/2)^{1/2}\sigma_z \tag{17}$$

and is used in eq. (13a).

3.2 Initial slumping and gravitational dominance

As the cloud collapses due to its own weight, the turbulence generated by the collapse controls the entrainment and the evolution of the cloud concentration and dimensions. We assume that the same behaviour occurs initially in a windy turbulent atmosphere and import the required equations from [1]. The cloud radius is found by integrating eq. (7a), which gives

$$\bar{R}^2-\bar{R}_0^2=2a_1\bar{t}/\pi^{1/2} \tag{18}$$

where $\bar{R}=R/l$, $\bar{R}_0=R_0/l$, and $\bar{t}=t/\tau$. Top entrainment controls the concentration within the core. The nondimensional bulk concentration $\bar{C}_b=C_b/C_0$ is equal to the inverse of the nondimensional bulk volume $\bar{V}=V/V_0$. These are expressed in [1] as

$$\begin{aligned}\bar{C}_b&=\bar{V}^{-1}\\ \bar{V}&=(1+c_1(H_0/D_0)^{1/3}\bar{t}^2)^{c_2}\end{aligned} \tag{19}$$

where $D_0=2R_0$. The calibration constants c_1 and c_2 are chosen so as to optimize the fit of eq. (19) to measured values of maximum surface concentrations within the core. With V and R established, the cylinder height is given simply by

$$H_g=V/\pi R^2 \tag{20}$$

where the subscript 'g' (for gravity) is a reminder that eq. (19) is a measure of cloud growth due to gravitationally induced turbulence and kinematic slumping. The Gaussian sigmas are given as

$$\sigma_{zg}=(2/\pi)^{1/2}H_g \tag{21}$$

$$\sigma_{rg}=a_3(R-R_0) \tag{22}$$

It is interesting to note that because the cloud grows radially outward as R and because σ_{rg} grows inward more slowly as a_3R ($a_3\approx 0.3$), the core radius continues to grow indefinitely. If eq. (22) is substituted into eq. (14), the asymptotic value of R_c/R is found to be 0.6.

3.3 Effect of ambient turbulence

Let us first consider the growth of a passive puff in the atmosphere. The theory of puff dispersion suggests that there are three successive stages of growth

in which $\sigma \propto t$, $t^{3/2}$, and $t^{1/2}$ as time progresses [9]. The theory of plume dispersion suggests that plume growth proceeds initially as t and then later as $t^{1/2}$. These theories were derived on the assumption of a homogeneous, stationary atmosphere. Since the real atmosphere deviates from these assumptions to varying degrees, these theories are only approximated to varying degrees. Unfortunately, because puff behaviour has been studied far less than plume behaviour, air pollution models generally use experimentally determined plume sigmas for both puff and plume applications.

As a dense cloud evolves and becomes dilute, its properties should asymptotically approach those of a passive puff. What is the appropriate time-dependent behaviour of this target puff? We know that the dense puff has been evolving due to self-generated turbulence and has been resisting intrusion of atmospheric turbulence. By the time that the cloud is transparent to atmospheric turbulence, it has a low height relative to its large radius. Since dispersion in the vertical direction has yet to be subjected to all scales of turbulence greater than H, it is far from the possible final $t^{1/2}$ dependence. Furthermore, experimental measurements of dispersion in lateral directions do not seem to approach $t^{1/2}$ dependence; plumes continue to grow as t, and puffs as t or $t^{3/2}$ [9]. At the intermediate time during which a dense puff makes a transition to a neutral puff, it seems reasonable that the asymptotic sigma growth rate should be proportional to t. This assumption is used in the present model development and model evaluation. However, modification of the model to use any other asymptotic sigma is very easy, as can be seen from eq. (32).

The transition to neutral density occurs as the cloud Richardson number Ri falls below a critical Richardson number Ri_c of order unity. This is evident from the definition of Ri as the ratio of cloud potential energy (which inhibits entrainment) to ambient turbulent energy (which stimulates entrainment). Representing the asymptotic or far field sigma as σ_{if}, a suitable asymptotic growth rate is simply

$$\frac{d\sigma_{if}}{dt} \approx u_i \quad Ri \ll Ri_c \tag{23}$$

which integrates to become $\sigma_{if} = u_i t$. Subscript 'i' refers to one of the 3 coordinate directions and may take values of x (or 1), y (or 2), and z (or 3). In nondimensional form,

$$\bar{\sigma}_{if} = \frac{u_i \tau}{l} \bar{t} = \frac{u_i \bar{t}}{q Ri_l^{1/2}} \tag{24}$$

where $\bar{\sigma}_{if} = \sigma_{if}/l$, u_i is the turbulence velocity component in the i-direction, and q and Ri_l are defined in eqs. (27) and (29). The determination of u_i is in itself a complex problem since it is slowly varying function of travel time for a puff and of averaging time for a plume. We will assume that the turbulence velocity

approaches a stationary limit and will allow u_i to adopt this limit. In practice, we can use an estimate or a measurement of u_i over, say, a 20-minute period.

At the other extreme, for small time, entrainment of air due to the action of atmospheric turbulence is inhibited by the large negative density gradient in the vertical direction within the cloud. We assume that the vertical gradient also inhibits entrainment in the radial direction due to the tendency of the pressure redistribution terms in the turbulent energy equation to maintain isotropic turbulence [10]. Equation (3) describes the rate of entrainment into a dense cloud due to mechanically generated ambient turbulence. Expanding this to include thermally generated turbulence, a more general expression for this near field component of entrainment or growth σ_{in} is

$$\frac{d\sigma_{in}}{dt}=\frac{Ri_c}{Ri}u_i \qquad Ri \gg Ri_c \tag{25}$$

where the proportionality constant Ri_c will be determined in order to optimize the fit of the model to the experimental data. The (bulk) Richardson number Ri is defined as

$$Ri=gH\Delta/q^2 \tag{26}$$

where

$$q^2=(u_1^2+u_2^2+u_3^2)/3 \tag{27}$$

is a measure of the ambient turbulent energy. Using eqs. (5a) and (7a), eq. (26) can be rewritten in terms of R (or $\bar{R}$) as

$$Ri=Ri_l/\pi\bar{R}^2 \tag{28}$$

where Ri_l is a characteristic Richardson number based on the length l and is given as

$$Ri_l=gl\Delta_0/q^2 \tag{29}$$

Because $\bar{R}^2$ is a simple function of $\bar{t}$, eq. (25) is readily integrable when eq. (28) is substituted for Ri. The integral then becomes

$$\bar{\sigma}_{in}=\frac{u_i\bar{t}}{qRi_l^{1/2}}\phi \tag{30}$$

where

$$\phi=\pi\frac{Ri_c}{Ri_l}\left[\bar{R}_0^2+\frac{a_1\bar{t}}{\sqrt{\pi}}\right] \tag{31}$$

upon using the substitution $q\tau/l=Ri_l^{-1/2}$. We now have expressions for the atmospheric component of cloud growth σ_{ia} in which $\bar{\sigma}_{ia}=\bar{\sigma}_{in}$ for $Ri \gg 1$ (which implies $\bar{t} \ll \mathrm{Ri}_l$) and $\bar{\sigma}_{ia}=\bar{\sigma}_{if}$ for $Ri \ll 1$ (or $\bar{t} \gg Ri_l$). An empirical combination which selects the correct function $\bar{\sigma}_{in}$ or $\bar{\sigma}_{if}$ as time advances is

$$1/\bar{\sigma}_{ia} = 1/\bar{\sigma}_{in} + 1/\bar{\sigma}_{if} \tag{32}$$

For the choice of $\bar{\sigma}_{if}$ as given in this paper by eq. (24), the above equation reduces to

$$\bar{\sigma}_{ia} = \bar{\sigma}_{if}\phi/(1+\phi) \tag{33}$$

For $\bar{t} \ll \mathrm{Ri}_l/Ri_c$, ϕ is small and the denominator approaches unity, allowing $\bar{\sigma}_{ia}$ to vary initially as $\bar{t}$ and then as $\bar{t}^2$. As $\bar{t}$ exceeds Ri_l/Ri_c, ϕ exceeds unity and $\bar{\sigma}_{ia}$ gradually changes to $\bar{\sigma}_{if}$ which describes the growth of a neutrally buoyant cloud. Alternate sigmas such as those recommended by Briggs in 1973 (see Hanna et al. [9]) could be used to replace σ_{if} in eq. (32).

Except for σ_m, we now have a full set of equations for the concentration field of the dense gas cloud in the atmosphere. If the maximum concentration given by eqs. (13) is divided by $C_0 = m_g/V_0$, then $\bar{C}_b$ is seen to be a function of $\bar{R}$ and $\bar{H}$ when $R_c > 0$ and a function of $\bar{\sigma}_i$ when $R_c = 0$. If we examine these nondimensional length variables, we see that they are functions of $\bar{t}$, H_0/D_0 (weakly), and Ri_l. In eq. (31), Ri_c remains as a calibration constant in order to optimize the fit of the predicted concentrations to the data.

The ratio u_i/q is of order unity and is practically constant. In practice, it is rare to have measurements of each u_i. In those cases for which the u_i are not known, we must rely upon an estimate of one component from a knowledge of the Pasquill–Gifford–Turner stability scheme or from the friction velocity u_* or the mixed layer scaling velocity w_*. Then, assuming that the ambient conditions are near neutral, approximate relations among boundary layer variables are [11]

$$u_1/u_* = u_2/u_* = 2, \quad u_3/u_* = 1.26 \tag{34}$$

from which

$$u_1/q = u_2/q = 1.13, \quad u_3/q = 0.68 \tag{35}$$

As long as we know one of the u_i, we can estimate q from eqs. (35) and use it in the expression for Ri_l. The above ratios for u_i/q can be used in eq. (24) for $\bar{\sigma}_{if}$ if the individual u_i have not been measured. Other initial conditions which must be known in order to evaluate the dimensional quantities of concentration, length, and time are V_0, ρ_0/ρ_a, H_0/D_0, and M_g.

3.4 Effect of molecular diffusion

Molecular diffusion will be important only in cases when the initial gas volume is small or if the atmosphere is calm. If the cloud height is only a few centimetres and the external turbulence is small, then eventually cloud growth in the vertical direction due to molecular diffusion will become important. The one dimensional time dependent diffusion equation has as a solution a Gaussian distribution with a characteristic diffusion distance given by [12]

$$\sigma_m^2 = 2D_m t \tag{36}$$

The diffusivity of air is about 1.5×10^{-5} m^2 s^{-1}. The diffusivity of a dense gas cloud will be lower initially but will tend toward that of air as air is entrained.

4. Cloud acceleration and drift

If the near field, the cloud accelerates from zero velocity up to a steady value. The acceleration is proportional to the wind speed and inversely proportional to the cloud mass. The determination of the cloud position is difficult without a good acceleration and drift model and deteriorates as the cloud mass increases. Of course, the exact position becomes less important as mass increases if the radial extent of the cloud far exceeds the drift distance.

The force which accelerates the cloud is a drag force of the atmosphere upon the cylinder. Two drag mechanisms may be important. One is caused by the entrainment of ambient momentum into the cloud. The other is caused by wind shear and wake formation which together can be referred to as form drag. We hypothesize that form drag is responsible for the initial motion and that momentum entrainment quickly becomes dominant. In the interests of simplicity, we will concentrate on a quantitative description of momentum entrainment, and a qualitative assessment of form drag. This is convenient since the role of entrainment is an essential component of this paper.

A bulk model for the rate of change of cloud mass is readily expressed as being equal to the mass entrainment rate through the top of the cylindrical cloud. Assuming that ambient mass of density ρ_a and ambient momentum of density $\rho_a U$ are entrained with the same velocity v_e, the rate of change of cloud mass ρV and cloud momentum $\rho U_c V$ are given by

$$\frac{d}{dt}(\rho V) = \rho_a v_e \pi R^2 \tag{37}$$

and

$$\frac{d}{dt}(\rho U_c V) = \rho_a U v_e \pi R^2 \tag{38}$$

where U_c and U are the cloud drift speed and wind speed, respectively. The above equations can be combined to give

$$\rho V \frac{dU_c}{dt} = (U - U_c)\frac{d(\rho V)}{dt} \tag{39}$$

Assuming U to be uniform and constant, eq. (39) for the cloud speed U_c integrates easily to become

$$U_c = U\left(1-\frac{\rho_0}{\rho}\frac{V_0}{V}\right) \approx U\left(1-\frac{1}{\bar{V}}\right) \tag{40}$$

The evolution of the product ρV is readily estimated from the expression for $b=b_0$ (following eqs. (7)) and V from eqn. (19). However, it was found adequate to simply ignore the dependence of U_c upon ρ_0/ρ. Since ρ_0/ρ increases in time from 1 to ρ_0/ρ_a, ignoring it causes U_c to be overestimated. The direction of the error (and hopefully the degree) is acceptable since we have ignored the effect of form drag in accelerating the cylinder. Since $U_c = ds_c/dt$, the integral of eq. (40) determines the position s_c of the cloud centre of mass. Of several approximate integrals which were found for this equation, the one which agrees best with the data is the very simplest, i.e.,

$$s_c = U_c t \tag{41}$$

where U_c takes on the local cloud velocity as given by eq. (40). Equation (41) is an overestimate of the position s_c as given by the exact integral of eq. (40). However, as argued above, this may also compensate for ignoring other drag components acting on the cylinder.

An improvement over a constant uniform wind assumption is a logarithmic wind variation in the vertical direction. If the wind speed U_R is known at a reference height z_R, then the wind speed U_H at the cloud height H is given by

$$\frac{U_H}{U_R} = \frac{\ln(H/z_0)}{\ln(z_R/z_0)} \tag{42}$$

where z_0 is the roughness height. A reasonable mean speed for the wind surrounding the cloud and an asymptotic drift speed for the cloud is some fraction of U_H, i.e.,

$$U = c_3 U_H \tag{43}$$

This expression for the local ambient wind speed can be used in eqs. (40) and (41) to calculate the local cloud speed U_c and locations s_c during and following acceleration. The universal constant c_3 was found to be 0.58 by comparing the model to Thorney Island data (Section 7.4).

5. Experimental data

Experimental data are essential ingredients of model design. They assist in three ways: (1) A plot of the data will often suggest an explanation of the physical processes which dictate the distribution of the data, (2) If there are several competing models to explain the data distribution, a comparison with data should select the preferred model, (3) The accuracy and suitability of the preferred model can be determined by comparing it to data.

The data used in the present model development and evaluation come from

4 sources. Full scale field studies were done at Thorney Island, U.K. and Porton Down, U.K. Laboratory studies were done at the University of Arkansas and at Colorado State University in the U.S.A.

5.1 University of Arkansas laboratory study (1983–1984)

This study was carried out by Havens and Spicer [13]. They studied the collapse of a cylindrical cloud of freon–air mixtures in a closed room with no ambient wind or turbulence. The initial volumes were 34, 54, 135, and 535 litres; initial specific gravities were 2.16, 2.91, and 4.19; initial height/diameter ratios were 0.4, 1.0, and 1.57. There was a total of 67 releases. Concentrations were measured continuously at several radial and vertical receptors. We have abstracted the maximum disk concentrations at the lowest receptors following the passage of the torus. These data provide us with data at an extreme Richardson number, i.e., $Ri = \infty$. This was the first data set used in the development of the present model and was used to calibrate the gravitational collapse behaviour [1].

5.2 Thorney Island full scale study (1982–1984)

This study examines the dispersion of large freon–air mixtures having initial volumes up to 2000 m^3. The objectives and preliminary results are described by McQuaid [14]. The data which we use are maximum concentrations occurring at the lowest level (0.4 m) of each of several towers downwind of the cylindrical source. The data are contained in 16 reports, each describing the initial conditions and meteorological and concentration measurements of an experiment. The 16 experiments are referred to as Trials 4–19. Of these, Trials 4, 5, 10, and 11 had insufficient data and are not used in the present paper. The remainder are used to develop and calibrate the model of entrainment due to ambient turbulence and the model of cloud drift. Initial conditions include measured values of U_R and u_1, u_2, and u_3.

5.3 Porton Down full scale study (1976–1977)

These studies are described in a three-part report by Picknett [15]. Each experiment consists of a release of 40 m^3 of a freon–air mixture over terrain of varying roughness and slope. Continuous concentration measurements are available from a very sparse network of samplers located usually on arcs 25 and 50 m from the source. For some experiments, a portable monitor was located several hundred metres downwind, near the expected cloud centreline. The wind speed at 2 m and the friction velocity u_* are available for each experiment; turbulence data for u_3 are available for some. There was a total of 42 releases with varying degrees of success. We have used data from 30 of these experiments to compare with the concentration and drift models.

5.4 Colorado State University wind tunnel study (1980–1982)

Of the 4 experimental studies, this one [16] has the smallest release volumes of 35, 165, and 450 cm^3. Wind speeds of 0.2, 0.4, 0.6, and 1.0 m s^{-1} are set at a height of 10 cm. Using a logarithmic wind profile and the tunnel roughness height of 0.024 mm, the friction velocity and turbulent velocities are estimated. Twelve runs are used, each having about 10 downwind receptors at a height of 2 mm. The shape of the initial volume is not a vertical cylinder like the above studies but is rather a half cylinder sliced through the axis of symmetry and lying on the flat side. The effective initial ratio of H/D is 0.5. Initial density ratios are all 4.17. The data are compared with concentration and drift model predictions and are also used to estimate the effect of vertical growth due to molecular effects in addition to turbulence. The concentration data which are presented are ensemble averages of peak concentration, each calculated from five quasi-identical runs.

6. Comparison of model results with experimental data

In this paper, we are concerned solely with bulk properties, i.e., the maximum concentration in the cloud (eqs. 13) and the downwind location of its centre of mass (eq. 41). We will examine first the maximum concentration and its dependence on time and characteristic Richardson number Ri_l using the Thorney Island data. The data are instantaneous measurements of concentration whose averaging time corresponds to that of the measuring instrument, i.e., about 1 s. A plot of measured concentration vs. time shows the data to be very irregular (Fig. 1). What we must bear in mind is that if the trial could be repeated a large number of times for the same initial conditions, a smooth distribution of points would appear for $\bar{C}$ vs. $\bar{t}$, with a well defined mean and standard deviation. Identical field experiments cannot be replicated, for reasons of cost as well as because of the capricious nature of meteorology. Any algebraic model for $\bar{C}$ vs. $\bar{t}$ can only represent the mean of the distribution. Consequently, with a small number of measurements, it is often difficult to get meaningful agreement between model and measurements.

The starting point for the model uses the equation of Section 3.2 where the calibration constants are similar to those in [1]. These are $c_1 = 0.05$, $c_2 = 0.5$, $a_1 = 1.16$, and $a_3 = 0.35$. The new equations are in Section 3.3 and have a single constant Ri_c to be determined. This critical Richardson number will be chosen so that the model makes the correct transition from the 'gravitational' mode to the 'atmospheric' mode in accordance with the behaviour of the data.

6.1 Thorney Island Trials 9 and 18

Data from two Trials are plotted in Fig. 1. If the mean path of all the decay curves from all the Trials were plotted, it would be obvious that they are stratified by the Richardson numbers Ri_0 or Ri_l. These characteristic numbers are

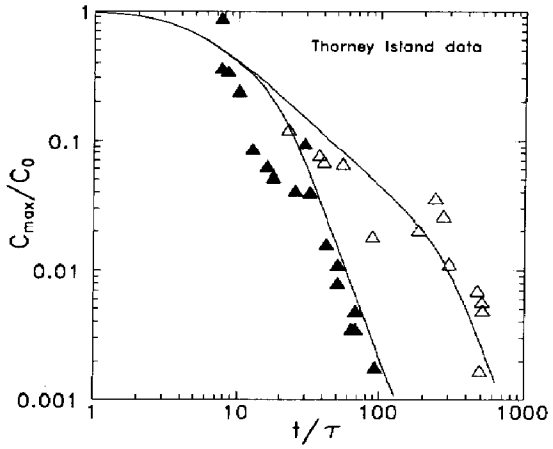

Fig. 1. Maximum concentration vs. time within a drifting cloud for two Thorney Island Trials having different characteristic Richardson numbers Ri_l. Trial 9: $Ri_l = 3870$ (△), Trial 18: $Ri_l = 115$ (▲).

proportional to H_0 and l, respectively. Because $H_0/D_0 \approx 1$ for these data, Ri_0 and Ri_l are proportional for the Thorney Island data. In general, Ri_l is the more important scaling parameter since only it appears in the cloud dimension $\bar{\sigma}_{ia}$ (eq. 33). Also eq. (28) shows that Ri begins as Ri_0 but soon becomes independent of H_0 as time progresses, i.e., it forgets its initial value.

The initial conditions in all Trials differ in wind speed, turbulence, volume, and density ratio. Plotted nondimensionally, these variables are absorbed into the new C and t coordinates such that the only remaining parameter is Ri_l. The Workbook of Britter and McQuaid [17] has a similar analysis in which C/C_0 is a function of x/l and Richardson number based on U and l. This is true only if $q \propto U$ as is the case in neutral conditions but does not hold for unstable conditions.

If data from all the trials were plotted on Fig. 1, the scatter of overlapping data would make interpretation difficult. Instead, we have chosen only two trials with significantly different Richardson numbers. For Trials 9 and 18, $Ri_l = 3870$ and 115, respectively. The differences in Ri_l are due mainly to differences in q^2, i.e., stable conditions during Trial 9 and neutral conditions during Trial 18. The larger Ri_l of Trial 9 implies that the cloud has a larger initial stability and will require a longer time $\bar{t}$ before Ri falls to Ri_c. The value of Ri_c which produced the best model-data agreement was 0.05. For the Porton Down data, it was 0.2. As a compromise, we will use $Ri_c = 0.1$ for all runs in this paper. The resulting model curves in Fig. 1 show reasonable agreement with the data. Initially, we assumed that the breakpoint in the slope of the model (or data) was the transition point from the dense slumping behaviour to the neutral Gaussian behaviour. The slopes change from -1 to -3 as would be expected. Upon examining the values of Ri, σ_{zg}, and σ_{za} in the numerical printout, it was noted that the breakpoint occurred when $\sigma_{za} = \sigma_{zg}$ at a time t_z. At this point, Ri

is still larger than Ri_c and the core of radius R_c still exists. Since σ_{za} was growing as t^2 (eq. 30), and since R^2 was growing as t (eq. 18), then from eq. (13a), the concentration would fall as t^{-3}. The breakpoint t_z then corresponds to the time at which ambient turbulence begins to dominate the vertical entrainment process.

6.2 Stratification by Richardson number Ri_l using all data

According to the model results, the core did not vanish nor did Ri drop below Ri_c for any of the Thorney Island Trials. This means that the transition from gravitationally controlled dispersion to Gaussian dispersion is a long and gradual process. Numerical output from the model suggests that the core radius R_c vanishes at about the same time that Ri falls below Ri_c. The time t_c when this occurs can be estimated from eq. (28). This second breakpoint is clearly visible on the model solutions for $Ri_l = 10$ and 100 in Figs. 2. It occurs as the concentration model changes from eq. (13a) to eq. (13b). The previous breakpoint occurs at time t_z found by equating σ_{zg} and σ_{za}. A third time of interest is the time t_ϕ when ϕ grows to unity in eq. (33). This is the time beyond which there is a gradual transition to a Gaussian distribution. Solving for all these times, we then find that

$$\bar{t}_z \approx 0.15 \frac{Ri_l^{3/4}}{Ri_c^{1/2}}, \qquad \bar{t}_c \approx 0.25 \frac{Ri_l}{Ri_c}, \qquad \bar{t}_\phi \approx 0.5 \frac{Ri_l}{Ri_c} \tag{44}$$

The times $\bar{t}_\phi$ are plotted on Fig. 2(d).

The nondimensional form of the model shows that $\bar{C}$ is a function of $\bar{t}$ and Ri_l, and is a very weak function of H_0/D_0. In plotting model results in Figs. 2, we assume that the aspect ratio $H_0/D_0 = 1$. (There is very little change in the curves if the aspect ratio is changed by an order of magnitude to 0.1). Six values are given to Ri_l ranging from 1 to 10^5. As a qualitative means of judging the model performance, data from all four experiments are plotted as well. To examine the dependence upon Ri_l, each of Figs. 2 contains only those data whose initial Ri_l vary by one order of magnitude. The range is indicated by the solid lines. Fig. 2(a) contains the lowest group of Ri_l, ranging from 10 to 100, in which the solid lines enclose the data reasonably well. The two breakpoints (where the slope changes), located at times t_z and t_c, are visible on the curves labelled by $Ri_l = 10$ and 100. The increase in slope beyond the second breakpoint occurs as the core radius R_c vanishes. The concentration equation (13b) takes over from eq. (13a). The increase in slope is due to the σ_{ia} which have a t^2 dependence but which are gradually changing to t. The data are not sufficiently numerous or accurate to know whether the second breakpoint is real or just a function of this particular model.

There are many more data in the next higher range in which $100 < Ri_l < 1000$ (Fig. 2b). The scatter is large, especially for the Porton data. The model tends to overpredict the concentrations for smaller values of $\bar{t}$. The trend is similar

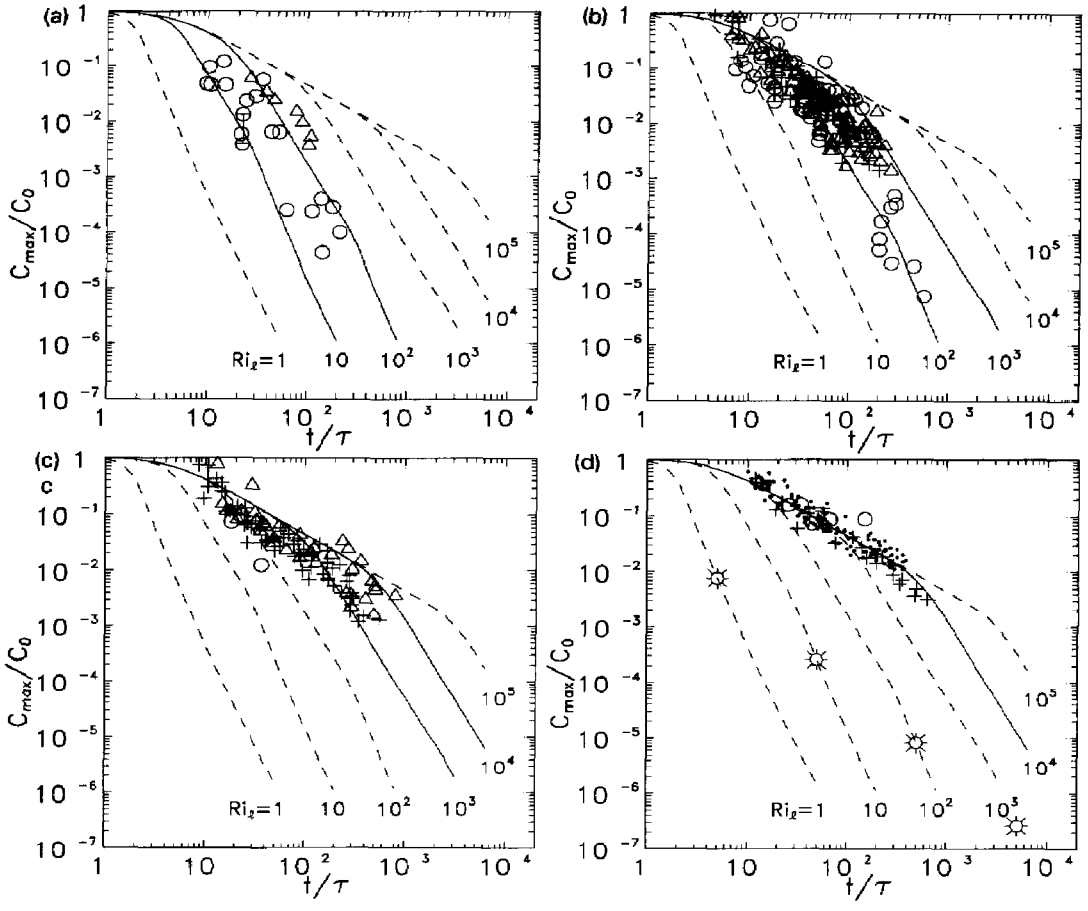

Figs. 2. Maximum concentration vs. time. Data are from Havens and Spicer (●), Meroney and Lohmeyer (+), Thorney Island (△), and Porton Down (○). Ranges of characteristic Richardson numbers in each Figure are: (a) $10 < Ri_l < 10^2$, (b) $10^2 < Ri_l < 10^3$, (c) $10^3 < Ri_l < 10^4$, and (d) $Ri_l > 10^4$. The symbol (☼) marks the time t_ϕ at which $\phi = 1$ (eq. 44).

for the next higher group of Ri_l (Fig. 2c), with the model continuing to overpredict at lower values of $\bar{t}$. Results from the most stable clouds are plotted in Fig. 2(d) and include values of Ri_l ranging from 10^4 to infinity. The Havens and Spicer data [13] have infinite Ri_l since the ambient turbulence is negligible. The Meroney and Lohmeyer experiments [16] have the smallest initial volumes. They do not seem to be significantly affected by molecular diffusion as the results are within the normal range of scatter of the other data.

The model seems to do a reasonable job in explaining the dependence of concentration $\bar{C}$ upon $\bar{t}$ and Ri_l. The accuracy of the solutions will be discussed in Section 7. We know that the dense gas solutions converge to Gaussian solutions as t increases. The Gaussian solution plots as a single line using its natural nondimensional coordinates whereas it retains an additional dependence upon Ri_l using the coordinate t/τ. Using a nondimensional time of $\bar{t}_n = t/\tau_n$ where $\tau_n = l/q$, the Gaussian solution can be written as

$$\bar{C}=\frac{2}{(2\pi)^{3/2}\bar{\sigma}_x\bar{\sigma}_y\bar{\sigma}_z+2} \tag{45}$$

where

$$\bar{\sigma}_i=\frac{\sigma_i}{l}=\frac{u_i}{q}\bar{t}_n \tag{46}$$

The possibility of a mixed layer of limited height is ignored in this treatment. The relation between τ and τ_n is $\tau_n^2=\tau^2 Ri_l$. The dense gas solutions on Figs. 2(a–d) and the Gaussian solution are plotted in Fig. 3 as functions of $\bar{t}_n$ and Ri_l. The dense gas solutions are seen to converge less rapidly to the Gaussian solution as Ri_l increases. Figs. 2(a–d) are useful for analysing dense gas behaviour because they stratify the data conveniently as a function of Ri_l. Figure 3 compresses the dense gas portion of the cloud's evolution but shows that for $\bar{t}_n$ beyond 10, the maximum concentration $\bar{C}$ does not vary by more than an order of magnitude above the Gaussian value, regardless of the value of Ri_l.

The use of a graph such as Fig. 3 offers a reasonably way to estimate the maximum concentration within an initially dense puff as it travels in time. It would be interesting to add the mixed layer depth as a parameter. Note that the concentrations are double valued as a function of Ri_l. Around $t/\tau_n \approx 1$, for example, the concentration increases as Ri_l increases from 0 to 1 because the increased stability dampens turbulence and entrainment. Then as Ri_l increases further, the concentration decreases because of the enhanced turbulence and entrainment due to gravitational collapse.

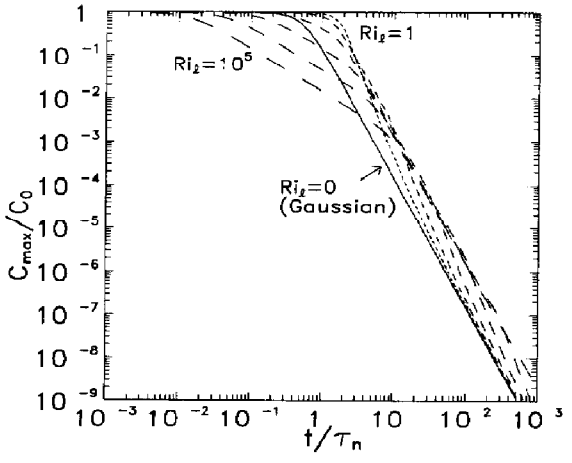

Fig. 3. Maximum concentration vs. time for a variety of dense clouds and a neutral density cloud ($Ri_l=0$) using the natural time scale τ_n of the neutral density cloud.

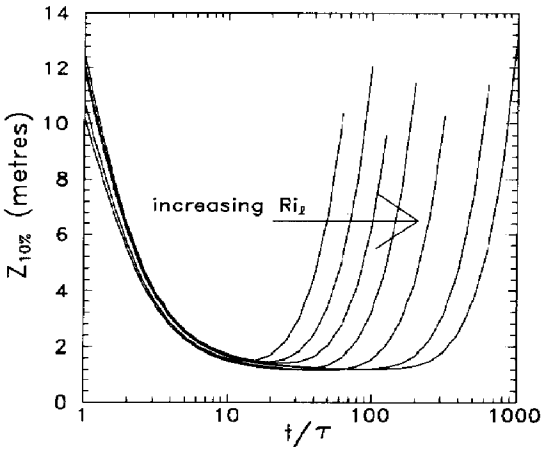

Fig. 4. Predicted heights at which the cloud concentration falls to 10% of the ground level concentration, plotted against time. They are produced using characteristic initial Richardson numbers of Ri_l=125, 190, 330, 525, 1000, 2000, and 4000. These Ri_l correspond approximately to Trials (14, 15, 18), (13, 16), 19, (6, 7, 8), 17, 12, and 9, respectively.

6.3 The 10% height

Once the maximum concentration is known from eqs. (13), it is a simple task to calculate the off-axis concentrations using eqs. (12). Off-axis concentrations are not of particular interest to this paper. However, Brighton [18] has used vertical measurements of the Thorney Island concentrations to estimate the height at which the concentration is 10% of the ground value. These heights ($Z_{10\%}$) are plotted against a nondimensional time $\bar{t}_B$ in Brighton's study which differs slightly from the $\bar{t}$ used in this study, i.e.,

$$\bar{t}_B = 4.6(H_0/D_0)^{2/3}\bar{t} \tag{47}$$

The 10% heights are calculated using the present model and are presented in Fig. 4. The present model has a minimum value of $Z_{10\%}$ of about 1.5 m whereas Brighton's estimated minima vary from 2 to 4 metres. Otherwise, the general behaviour of $Z_{10\%}$ as a function of Ri_l is the same.

7. Uncertainty

A model is an approximation of reality, and as such has a degree of uncertainty. Observations also have a degree of uncertainty. Since observations are usually the standard against which a model is evaluated, observational errors complicate the process of model evaluation.

An instructive analysis of uncertainty is given by Venkatram [19]. He suggests that the major contributors to uncertainty are (1) errors in model physics, (2) errors in model inputs, (3) errors in observations, and (4) inherent uncertainty. Most laboratory and field studies generate high quality data under well defined initial and boundary conditions which should minimize error #3.

Some of these data are used as input to the model (meteorology, initial volume and density, etc.) and should minimize error #2. All these errors will be discussed in more detail in the following sections.

We are interested in the accuracy of the modelled cloud radius, height, drift distance, and concentration. These items are interrelated and so most effort will be spent on evaluating a single item, i.e., the concentration predictions. The concentrations are referred to as instantaneous but in reality are averaged over a time interval of about 1 s.

7.1 Observational and inherent uncertainty

In the four experimental studies which are referred to in this paper, we assume that the instrument error is negligible. Since we are interested in peak concentrations, it is essential for the monitors to be located along the cloud centre-line. In the two full-scale studies, it is more difficult to be assured of this, since the wind is capricious and the monitor network is of limited resolution. The monitor location can only err in one direction, i.e., off the peak or towards lower concentrations. We assume that observational errors may be biased towards lower concentrations.

Inherent uncertainty is due to phenomena beyond our control or beyond our ability to resolve in a model, i.e., atmospheric turbulence. It can be studied by releasing a pollutant repeatedly under 'identical' initial conditions in a laboratory study. Observations show that the concentration traces at the same receptor always differ from one another. After a large number of quasi-identical experiments, it becomes evident that the traces form a distribution. A minimal but often adequate description of a distribution is afforded by the first two moments of the concentration, i.e., the mean and standard deviation. The distribution of particular interest in this study is that of the instantaneous concentration maxima at a given receptor. The average of the maxima is the ensemble mean; the standard deviation is the unresolvable or inherent uncertainty. By defining the distribution, the probability of any concentration occuring at the receptor can be estimated.

Inherent uncertainty is independent of the model. It is a measure of our inability to completely specify or control the initial state and boundary conditions of any experiment. The best that we can do is to define mean initial and boundary conditions (wind speed and direction, etc.). Let us label these resolvable parameters collectively as α; the remaining unresolvable turbulent parameters are labelled as β (Venkatram [19]). Although it is virtually impossible to repeat an experiment in the atmosphere having constant α, such an experiment can easily and cheaply be repeated in the laboratory. For arbitrary conditions α and β, a single concentration measurement $C_o(\alpha,\beta)$ can be represented as

$$C_o(\alpha,\beta) = C_o(\alpha) + c_{ob}(\alpha) + c_{oi}(\alpha,\beta) \tag{48}$$

The term $C_0(\alpha)$ is the ensemble average (averaged over β) of actual peak concentrations, and $c_{ob}(\alpha)$ is a mean observational error which biases the observation. The most likely bias is to measure a concentration below the peak value. The random component or inherent uncertainty is $c_{oi}(\alpha,\beta)$. (In this section, C_o is the observed concentration and should *not* be confused with the initial concentration C_0 mentioned in earlier Sections.) The α-parameters are time-averaged long enough so that their values are quasi-stationary. Although the boundary conditions are quasi-steady, the growth and translation of a gaseous puff are not. From the time-varying instantaneous concentrations at a fixed receptor, time-averaged concentrations or dosage calculations can be made.

A single experiment allows us to measure $C_o(\alpha,\beta)$ at each receptor but the results have limited meaning. Several experiments in which the α are fixed allow us to determine the distribution of $C_o(\alpha,\beta)$. The observed ensemble mean $C'_o(\alpha)$ differs from the true ensemble mean $C_o(\alpha)$ by the bias error $c_{ob}(\alpha)$. The observed ensemble mean, found by averaging over all β, is

$$C'_o(\alpha) = \langle C_o(\alpha,\beta) \rangle_\beta = C_o(\alpha) + c_{ob}(\alpha) \tag{49}$$

from which the observed variance is

$$\sigma_c^2(\alpha) = \langle [C_o(\alpha,\beta) - C'_o(\alpha)]^2 \rangle_\beta = \langle c_{oi}^2(\alpha,\beta) \rangle_\beta \tag{50}$$

It is reasonable to assume that the random component $c_{oi}(\alpha,\beta)$ attributes its magnitude to the ensemble mean $C_o(\alpha)$ and its fluctuations to a purely random function $a_{oi}(\beta)$ of order unity, i.e.,

$$c_{oi}(\alpha,\beta) = a_{oi}(\beta) C_o(\alpha) \tag{51}$$

Keeping α constant, and averaging over all β, eq. (50) becomes

$$\sigma_c^2(\alpha)/C_o^2(\alpha) = \langle a_{oi}^2(\beta) \rangle_\beta = I'^2 \tag{52}$$

where I' is the normalized inherent uncertainty in the measured concentration. The ratio of the standard deviation to the mean is a measure of the relative error in a concentration estimate. In statistical literature, it is also referred to as the coefficient of variation or coefficient of dispersion. Since it was assumed that $a_{oi}(\beta)$ was not a function of α, I' should also be constant for all α.

7.2 Model uncertainty

A concentration estimate is a function of the physics contained in the model. Complex models treat turbulence explicitly, using random walk or large eddy simulation techniques. Simpler models are functions solely of mean or smoothed properties and as such provide an estimate of the ensemble average concentration $C_o(\alpha)$. The model concentration is unchanged if the smoothed input parameters α are unchanged and can be represented as $C_m(\alpha)$. The model in the present paper estimates instantaneous concentrations at any point within a

finite dense gas cloud. In general, the model concentration will differ from the observed ensemble by a model bias $c_{mb}(\alpha)$ which is a function of α, i.e.,

$$C_m(\alpha) = C_o(\alpha) + c_{mb}(\alpha) \tag{53}$$

The smallness of the model bias determines the accuracy of the model in predicting the ensemble average.

7.3 Model evaluation

At this point, it appears that the evaluation of the model output $C_m(\alpha)$ should be done by comparing it to the ensemble mean of the observed concentrations $C_o(\alpha)$. There are two problems outstanding. Firstly, we are rarely able to collect enough data with constant α such that we can calculate the ensemble mean. Such an approach would render useless the enormous collection of $C_o(\alpha,\beta)$ data in which α varies from run to run. Therefore we will make a comparison between $C_m(\alpha)$ and $C_o(\alpha,\beta)$ and attempt to interpret the results. Secondly, there is a variety of opinions on how the comparison should be made. An American Meteorological Society (AMS) workshop on model performance evaluation [20] recommends the basic statistical variable to be the concentration difference $C_o - C_m$. A more recent AMS publication on emergency response recommends the comparison to be made using the ratio C_m/C_o [21]. In the latter approach, the goal is to determine the distribution of the ratio from which useful statistics can be generated. Since concentrations may vary over many orders of magnitude in any experiment or industrial accident, the concentration difference $C_o - C_m$ will also vary over many orders of magnitude, even for a good model. The ratio method, on the other hand, should transform all the data to order unity from which useful statistics should result. The ratio method is used in the present paper.

The ratio $\mathscr{R}' = \mathscr{R}(\alpha,\beta) = C_m(\alpha)/C_o(\alpha,\beta)$ is one element of a distribution whose properties we hope to define. Using eqs. (48) and (53) in the ratio and assuming all the error terms to be small, the denominator of $\mathscr{R}(\alpha,\beta)$ can be expanded as an infinite series. Retaining only first order terms, we have

$$\mathscr{R}(\alpha,\beta) \approx \left(1 + \frac{c_{mb}(\alpha)}{C_o(\alpha)}\right)\left(1 - \frac{c_{ob}(\alpha)}{C_o(\alpha)} - \frac{c_{oi}(\alpha,\beta)}{C_o(\alpha)}\right) \tag{54}$$

If $C_o(\alpha,\beta)$ is measured many times under identical conditions α, the ensemble mean of the ratio can be calculated directly from the data, or can be expressed analytically as

$$\mathscr{R}(\alpha) = \langle \mathscr{R}(\alpha,\beta) \rangle_\beta \approx 1 + \frac{c_{mb}(\alpha)}{C_o(\alpha)} - \frac{c_{ob}(\alpha)}{C_o(\alpha)} \tag{55}$$

Using eqs. (54) and (55), $\mathscr{R}(\alpha,\beta)$ can be approximated by

$$\mathscr{R}(\alpha,\beta) \approx \mathscr{R}(\alpha) - \mathscr{R}(\alpha)\left(\frac{c_{oi}(\alpha,\beta)}{C_o(\alpha)}\right) \tag{56}$$

Using eqs. (51), (52), and (56), the variance of $\mathscr{R}(\alpha,\beta)$ for fixed α is

$$\sigma^2_{\mathscr{R}'}(\alpha) = \langle [\mathscr{R}(\alpha,\beta) - \mathscr{R}(\alpha)]^2 \rangle_\beta \approx \mathscr{R}^2(\alpha) I'^2 \tag{57}$$

Since α has been held constant, the only source of uncertainty at this point is the inherent uncertainty of turbulence, as shown in eq. (57). Knowing the mean and variance of $\mathscr{R}(\alpha,\beta)$ for specific conditions α, we have an estimate of the distribution of $C_o(\alpha,\beta)$ for a given model estimate $C_m(\alpha)$.

It is neither practical nor possible to make repeated measurements for all combinations of α. What are the implications then for the data from a full-scale field study in the atmosphere in which conditions α are rarely repeated? The transformed data $\mathscr{R}(\alpha,\beta)$ can be considered to be a very sparse sample of a larger distribution in which both α and β are varying. If we now calculate the mean and variance using all data, averaging first over β and then over α, we find that

$$\mathscr{R} = \langle \mathscr{R}(\alpha,\beta) \rangle_{\beta,\alpha} = \langle \mathscr{R}(\alpha) \rangle_\alpha \tag{58}$$

and

$$\begin{aligned} \sigma^2_{\mathscr{R}'} &= \langle (\mathscr{R}(\alpha,\beta) - \mathscr{R})^2 \rangle \\ &= \langle (\mathscr{R}(\alpha,\beta) - \mathscr{R}(\alpha))^2 \rangle + \langle (\mathscr{R}(\alpha) - \mathscr{R})^2 \rangle \\ &\approx \langle \mathscr{R}^2(\alpha) \rangle I'^2 + \langle \mathscr{R}^2(\alpha) \rangle - \mathscr{R}^2 \end{aligned} \tag{59}$$

In practice, it is a straight-forward process to find the mean $\mathscr{R}$ and standard deviation $\sigma_{\mathscr{R}'}$ of all the ratios $\mathscr{R}(\alpha,\beta)$. The model can now be applied with some precision in environmental conditions similar to those of the calibrating experiment. Assuming that the observational errors $c_{ob}(\alpha)$ were negligible (eq. 49), then for an instantaneous concentration estimate $C_m(\alpha)$, we can estimate the true ensemble mean $C_o(\alpha)$ to be $C_m(\alpha)/\mathscr{R}$. The standard deviation of concentrations $C_o(\alpha,\beta)$ about $C_o(\alpha)$ is $C_0(\alpha)\sigma_{\mathscr{R}'}/\mathscr{R}$, providing the ratio $\sigma_{\mathscr{R}'}/\mathscr{R}$ is small relative to unity.

Rewriting eq. (59), we have

$$\underset{(T^2)}{\frac{\sigma^2_{\mathscr{R}'}}{\mathscr{R}^2}} \approx \underset{(I^2)}{\frac{\langle \mathscr{R}^2(\alpha) \rangle}{\mathscr{R}^2} I'^2} + \underset{(M^2+O^2)}{\frac{\langle \mathscr{R}^2(\alpha) \rangle - \mathscr{R}^2}{\mathscr{R}^2}} \tag{60}$$

The left side can be described as the normalized total variance T^2 in a concentration estimate. The first term on the right is the normalized inherent variance I^2. The remaining term combines the normalized variances M^2 due to

model imperfections and O^2 due to observational errors. Expressing eq. (60) in this alternate form, we have

$$T^2 = I^2 + M^2 + O^2 \tag{61}$$

In reality, for given α, there is a dense cloud having an ensemble mean peak concentration $C_o(\alpha)$ with a standard deviation $C_o(\alpha)I'$. Using a model to predict $C_o(\alpha)$ over a range of α increases the uncertainty in $C_o(\alpha)$ since the model performance (as well as observational errors) may vary with α. This uncertainty is expressed by the second term on the right side of eq. (60) (equivalent to M^2+O^2). In addition, the inherent uncertainty is modified slightly from I' to I. In eq. (60) I' or I express the uncertainty in specifying $C_o(\alpha,\beta)$; M and O express the uncertainty in specifying $C_o(\alpha)$. Hence the total standard deviation T describing the range of $C_o(\alpha,\beta)$ about $C_o(\alpha)$ is increased as given by eqs. (60) or (61).

In cases when $\sigma_{\mathscr{R}'}/\mathscr{R}$ is large, a normal distribution calculation for $C_o(\alpha,\beta)$ will contain negative concentrations. To avoid this, it is preferable to use log $\mathscr{R}'$ (base 10) or ln $\mathscr{R}'$ (base e) instead of $\mathscr{R}' = \mathscr{R}(\alpha,\beta)$ as the statistical variable. Both $\mathscr{R}'$ and log $\mathscr{R}'$ were used throughout the analysis. Judging from estimates of skewness (third moment) and kurtosis (fourth moment) as calculated by the SAS® software, the log $\mathscr{R}'$ variables are usually closer to a normal distribution than the $\mathscr{R}'$ variables. The observed concentration distribution can be derived from the mean and variance of log $\mathscr{R}'$ in the same way as for $\mathscr{R}'$. The means and standard deviations of the two distributions are simply related if the normalized standard deviation is small. Suppose A is a variable such that a typical instantaneous value is given by

$$A = \langle A \rangle + \delta A \tag{62}$$

where $\langle A \rangle$ is the mean, δA is the random component, and $\delta A/\langle A \rangle$ is small. By taking the logarithm of both sides, and expanding the right-hand side in terms of the small parameter $\delta A/\langle A \rangle$, one can show that

$$\langle \ln A \rangle \approx \ln \langle A \rangle \tag{63}$$

$$\mathrm{Var}(\ln A) \approx \mathrm{Var}(A)/\langle A \rangle^2 = (\sigma_A/\langle A \rangle)^2$$

where $\mathrm{Var}(A)$ is the variance of A.

7.4 Model evaluation results

The normalized standard deviation $\sigma_A/\langle A \rangle$ is a useful measure for comparing the relative uncertainty among distributions having different magnitudes of $\langle A \rangle$. Note that it is comparable to the standard deviation of the natural logarithm of A which one would expect to be independent of the magnitude of A. Table 1 contains a summary of the concentration results for the four data sets. The mean and standard deviation of $\mathscr{R}'$ and log $\mathscr{R}'$ are presented. These

TABLE 1

Summary of means and standard deviations for N values of the concentration ratio $\mathscr{R}' = \mathscr{R}(\alpha,\beta) = C_m(\alpha)/C_o(\alpha,\beta)$. (HS = Havens and Spicer, ML = Meroney and Lohmeyer, TI = Thorney Island, and PD = Porton Down)

Data	N	$\mathscr{R}$	$\sigma_{\mathscr{R}'}/\mathscr{R}$	$\langle \log \mathscr{R}' \rangle$	$\sigma_{\log \mathscr{R}'}$
HS	134	0.98	0.31	−0.027	0.132
ML	119	1.90	0.60	0.220	0.217
TI	123	1.14	0.59	−0.029	0.296
PD	84	2.93	0.96	0.283	0.416

are the minimum statistics which allow us to calculate the probability of exceeding a given concentration at a given location, assuming the distribution of $\mathscr{R}'$ or $\log \mathscr{R}'$ to be normal. The standard deviations in Table 1 are a measure of the uncertainty in our knowledge of a specific $C_o(\alpha,\beta)$ relative to the ensemble mean estimate of C_o.

The mean of the concentration ratio $\mathscr{R}'$ is similar to a bias calculation in that $\mathscr{R} > 1$ implies overprediction and $\mathscr{R} < 1$ implies underprediction. Here we see that $\mathscr{R}$ is close to unity for the Havens and Spicer (HS) data and for the Thorney Island (TI) data. Agreement with the HS data is not surprising since the model was calibrated to the data and describes the effects of gravitationally generated turbulence. This HS calibration worked quite well for the TI data during the slumping phase. In addition, the TI data were used to calibrate the model at the later stage when atmospheric turbulence becomes important. The uncertainty is larger using the TI data presumably because atmospheric conditions are much less uniform than laboratory conditions and because they contain additional influences (wind, ambient turbulence, etc.). Also, there is a 14% overprediction. One possible explanation is that some of the masts in the monitoring network may have missed the cloud centre (maximum) as it drifted by. Another is that the receptor, 40 cm above the ground, may have been too high to detect the maximum.

The remaining two data sets were not used to calibrate the model and so can serve as an independent judge of model performance. Unfortunately, they have some drawbacks which hinder this role. The model overpredicts by a factor of 2 relative to the Meroney–Lohmeyer (ML) wind tunnel data. The clouds, which are only a fraction of a litre initially, fall to a minimum height measured in millimetres. Molecular diffusion in the vertical direction probably dominates turbulent diffusion at this point and causes a volume growth greater than that predicted by the model, which neglects molecular diffusion. Consequently, observed concentrations are less than modelled concentrations. Uncertainty is comparable to that using the TI data.

Model performance deteriorates with respect to the Porton Down (PD) data.

The initial and boundary conditions are similar to those of TI, although the PD initial cloud volume V_o is 40 m^3 relative to the 2000 m^3 of TI. However, the much greater volume differences between the ML laboratory studies and the TI studies do not seem to cause a strong a difference in model performance. The large overprediction of $\mathscr{R}$ may be due to the very sparse monitoring network that simply fails to locate the central portion of the puff. In addition, the rougher surface may trap pockets of gas, causing a net loss of mass from the cloud. To determine the reasons for discrepancies would require a thorough examination of experimental conditions and results. The uncertainty $\sigma_{\mathscr{R}'}/\mathscr{R}$ is also much larger.

Figures 5 display the data that are summarized in Table 1. The figures give a qualitative assessment of the model performance. They also suggest the minimum criteria for a good model performance. These are:

(a) $\langle \mathscr{R}' \rangle = \langle C_m(\alpha)/C_0(\alpha,\beta) \rangle \approx 1$, averaged over all data.

(b) The local mean of $\mathscr{R}'$ is not a function of the choice of α (t/τ in this case).

(c) The local variance $\sigma^2_{\mathscr{R}'}(\alpha)$ is not a function of the choice of α (t/τ in this case).

(d) M and O are small relative to 1. The standard deviation I (or I') is not a problem since it is a property of nature and represents information as well as uncertainty once it is determined.

In general, it seems plausible that the local variance could be a function of α. In Figs. 5, the local variance of $C_m/C_o(\alpha,\beta)$ is fairly uniform over the range of

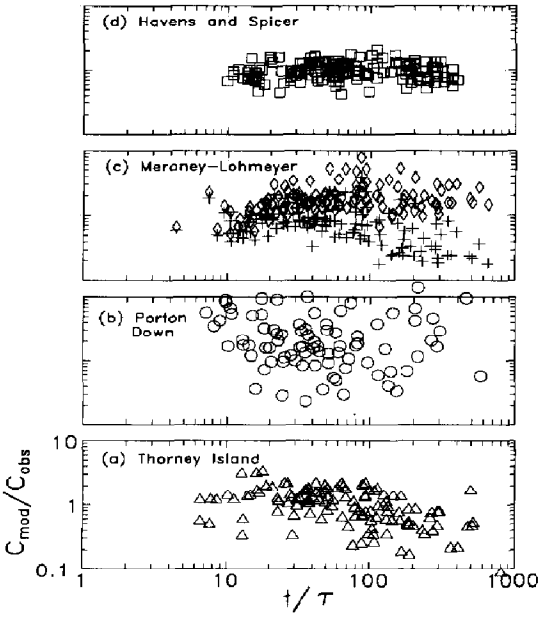

Figs. 5. The ratio of modelled to observed concentrations for several experiments. In (c), the model is run with (+) and without (◇) molecular diffusion.

t/τ. This simplifies the application of the model since a single variance can be used regardless of the value of α.

In the process of calibrating the model using the HS and TI data, calibration constants were chosen so as to satisfy criteria (a) and (b). There is no control over the variance except to maximize the quality of both the model and the data. A comparison with the TI data (Fig. 5a) shows that all the criteria are upheld reasonably well except for (b), i.e., there is a gradual decrease in the local mean of $C_m/C_o(\alpha,\beta)$ as t/τ increases. This is due primarily to the choice of Ri_c as 0.1, which is an compromise between the optimum values for the TI data (0.05) and the PD data (0.2). In retrospect, the TI data seem much better than the PD data and so more weight should be given to the former results. For example, if Ri_c is reduced, the transition to rapid cloud growth is delayed and model concentrations would be higher at larger times. This would improve agreement with criterion (b) for Fig. 5(a) but would increase the value of $\langle \mathscr{R}' \rangle$ further above unity (violating criterion (a). Criterion (b) is probably more important, however.

The variance is largest for the PD data (Fig. 5b). Even for small values of t/τ, where concentrations should be close to their initial values, the model grossly overpredicts. Using the ML data (Fig. 5c), the model fails conditions (a) and (b). If molecular diffusion is neglected ($\diamond$), the local mean begins below 1 and climbs to about 2. If we modify the model so as to allow additional vertical diffusive growth by molecular action as given by eqn. (36), the local mean (+) climbs to a maximum of 1 and then falls. This simple modification does not improve the performance.

The best performance occurs for the HS data of Fig. 5(d) and satisfies all four of the above criteria. However, the HS data conditions are rarely experienced in practice (zero wind, zero ambient turbulence).

Our goal is to be able to predict a distribution of real concentrations, given a model concentration. A real distribution is characterized by its mean and inherent uncertainty (C_o,I'). A predicted distribution is characterized by the mean and a broader uncertainty (C_o,T). The broader distribution results from the fact that the model does not predict the mean $C_o(\alpha)$ correctly over the entire range of α. In determining the total uncertainty T, we want to be sure that it is not augmented by bad data (observational errors). Which combination of $\mathscr{R}$, $\sigma_{\mathscr{R}'}/\mathscr{R}$ (Table 1) is most representative of the model for general application? For reasons expressed earlier, the TI data-model comparison probably indicates a reasonable relationship between model prediction and data reality. Because of the uncertainty in the estimates, we can be probably assume that $\mathscr{R} \approx 1.0$, $\sigma_{\mathscr{R}'}/\mathscr{R} \approx 0.6$, or $\langle \log \mathscr{R}' \rangle \approx \log \mathscr{R} \approx 0.0$, $\sigma_{\log \mathscr{R}'} \approx 0.3$.

7.5 Acceleration and translation

In Section 4, equations were developed for the acceleration of the dense cloud from rest. These were solved to yield simple expressions for the local cloud

speed U_c and downwind distance s_c. The only calibration constant c_3 in the drift model was found by comparing the model drift distance to the TI drift data. The comparison was made using the ratio method as before, where the statistical variable is defined as $\mathscr{R}(\alpha,\beta)=S_m(\alpha)/S_o(\alpha,\beta)$. The statistics are presented in Table 2 and are plotted in Fig. 6a. The triangles ($\triangle$) result from the use of eqn. (41) and show very good agreement with the data. The dots ($\bullet$) result from a simpler equation, $s_c=U_R t$, which assumes that the puff accelerates instantly to the constant wind speed measured at a 10 m high tower.

There were two restrictions applied to the choice of TI drift data:

(i) Twelve trials were used in the selection of peak concentration data. In addition, the time of arrival of the cloud centre of mass at the receptor was recorded. This was to be the time used for calibrating the model drift distance to the receptor distance. However, in three experiments (9, 12, 17), the concentration traces at the receptor were more highly skewed, making an estimate

TABLE 2

Summary of means and standard deviations for N values of the drift ratio $\mathscr{R}'=\mathscr{R}(\alpha,\beta)=S_m(\alpha)/S_o(\alpha,\beta)$. (HS=Havens and Spicer, ML=Meroney and Lohmeyer, TI=Thorney Island, PD=Porton Down)

Data	N	$\mathscr{R}$	$\sigma_{\mathscr{R}'}/\mathscr{R}$	$\langle \log \mathscr{R}' \rangle$	$\sigma_{\log \mathscr{R}'}$
ML	119	0.91	0.43	−0.101	0.259
TI	60	1.00	0.15	−0.005	0.070
PD	51	1.27	0.46	0.066	0.185

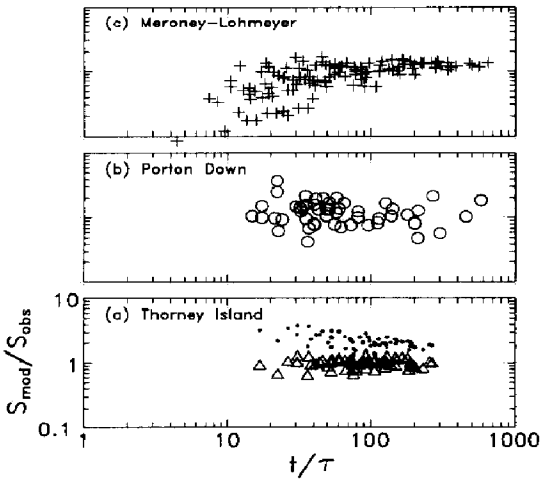

Figs. 6. The ratio of modelled to observed cloud travel distances for several experiments. In (a), a simpler model is also used, i.e., $s_c=U_R t$ ($\bullet$), in which U_R is a constant mean wind speed measured at 10 m above ground level.

of the centre of mass arrival time more difficult. Hence, these three experiments were dropped.

(ii) The second restriction was in the selection of downwind receptors. Only those receptors within ±15 degrees of the wind direction were used.

A further comparison of the modelled drift distance (eqn. 41) with measured distances is given in Table 2 and Figs. 6 using the PD and ML data sets. Again, because the TI data appear to be superior to the PD data, the normalized standard deviation of 0.15 is probably a good measure of the total uncertainty in applying eq. (41) for drift estimates over flat terrain.

7.6 Uncertainty components

The uncertainty components which are significant in the distribution of $\mathscr{R}(\alpha,\beta)$ are related to the total uncertainty T as in eq. (61). The uncertainties which are important in making error estimates associated with model calculations are inherent uncertainty I and model uncertainty M. To establish I, it is necessary to repeat an experiment several times, keeping α constant. This is feasible only for laboratory experiments. The inherent uncertainty I' for fixed α can be calculated from eqs. (52) or (57); the inherent uncertainty I (or I') for all α can be found from eq. (60). To establish the model error M, it is necessary that the observational errors O are negligible. We assume that the environmental conditions of the HS and ML experiments are well-controlled such that $O \approx 0$.

Table 3 contains some results from the HS data in which 34 identical runs were repeated. Because the receptor locations r_r were not identical for all runs, the number of repetitions N differs for each receptor. The initial conditions are $V_0=54.1$, $\rho_0/\rho_a=4.19$, and $H_0/D_0=1$. The 10 different receptor locations create 10 different α-conditions. The value of $\mathscr{R}(\alpha)$ is seen to increase as r_r increases, signifying a bias which is a function of α in the model. The value of $\sigma_{\mathscr{R}'}(\alpha)$ also increases with α. However, the ratio $\sigma_{\mathscr{R}'}(\alpha)/\mathscr{R}(\alpha)$ varies more

TABLE 3

Calculation of the mean and standard deviation of $\mathscr{R}(\alpha,\beta)=C_m(\alpha)/C_o(\alpha,\beta)$ and of $C_o(\alpha,\beta)$ for N repetitions of identical initial conditions at various radial receptors r_r using the Havens and Spicer laboratory data

Parameter	r_r (m)									
	1.00	1.50	1.80	2.00	2.20	2.40	2.60	2.90	3.50	4.10
N	24	16	6	18	9	6	18	10	9	8
$\mathscr{R}(\alpha)$	0.69	0.84	0.93	1.03	1.21	1.11	1.15	1.21	1.93	1.34
$\sigma_{\mathscr{R}'}(\alpha)$	0.08	0.10	0.11	0.12	0.25	0.14	0.21	0.25	0.48	0.46
$\sigma_{\mathscr{R}'}(\alpha)/\mathscr{R}(\alpha)$	0.11	0.12	0.11	0.11	0.20	0.12	0.18	0.21	0.25	0.35
$\sigma_c(\alpha)/C_o(\alpha)$	0.10	0.16	0.11	0.15	0.16	0.14	0.13	0.10	0.19	0.26

slowly. We had postulated that this ratio should be a constant, equal to I' as in eq. (57). We will take I' for the HS data set to be the mean of these 10 values, i.e., 0.18 ± 0.08. A second estimate of I' for each α is available directly from the measurements as in eq. (52) and are printed in the final row of Table 3. The mean of these values is 0.15 ± 0.05.

We would also like to test the value of eq. (60) in evaluating uncertainty components I', I, and M for the same identical HS runs (assuming $O=0$). The results are shown in Table 4. Note that I' is somewhat larger than the previous two estimates. The lack of agreement in the estimates of I' is probably due to the gross assumptions that the uncertainty terms are small and that I' is independent of α.

Meroney and Lohmeyer [16] repeated each experiment five times over on the average. For three initial volumes, four non-zero wind speeds, and about 10 receptors, they tabulate the mean concentration and standard deviation for each receptor. Using eq. (52), these provide a large number of estimates of I' which are averaged to give 0.25 ± 0.12. Using eq. (60), $I' \approx 0.34$. The remaining uncertainty estimates are given in Table 4. Uncertainties are larger in the ML results possibly because of additional independent variables α such as non-zero winds and molecular effects.

Note that T in Table 4 differs from $\sigma_{\mathscr{R}'}/\mathscr{R}$ in Table 1 for the HS and ML data. The HS standard deviations differ for two reasons:

(1) The data used for Table 1 were abstracted by the author from the HS data traces for an earlier paper [1]. They differ slightly from the tabulated peak concentrations reported by Havens and Spicer [13]. In addition, the data used for Table 4 is a subset of the latter data set.

(2) It was realized late in the study that the ML concentration data [16] were measures of ensemble means $C_o(\alpha)$ rather than single measurements $C_o(\alpha,\beta)$. Knowing $C_o(\alpha)$ and $\sigma_c(\alpha)$ for 119 ensembles, the additional variance due to the $\sigma_c(\alpha)$ was added to give a larger value of T in Table 4.

An interesting and possibly coincidental observation from the laboratory results is that the relative magnitude of the components I, M, and T within

TABLE 4

Summary of the approximate results for inherent uncertainty (I' and I), model uncertainty (M), observational uncertainty (O), and total uncertainty (T) in concentration estimates based upon the four experimental studies

Data	I'	I	M	O	T
HS	0.20	0.18	0.30	0.0	0.36
ML	0.34	0.40	0.60	0.0	0.72
TI	-	-	-	-	0.59
PD	-	-	-	-	0.96

each experiment is the same. They indicate that inherent uncertainty contributes 32% of the variance and model uncertainty contributes 68%.

The full scale atmospheric studies do not allow for repeated identical runs to estimate I or M. The only uncertainty statistic available is total uncertainty T which is 0.59 for TI data and 0.96 for PD data. On the basis of the 4 studies and putting more weight on the TI results than on the PD results, we suggest that the dense gas model can be used to predict the ensemble mean and uncertainty of peak concentrations reasonably well assuming that $\mathscr{R} \approx 1$ and $\sigma_{\mathscr{R}'}/\mathscr{R} \approx 0.6$.

A further source of error which may arise during applications is input error or source uncertainty S. For small uncertainties in source conditions or meteorological variables, S can be found by differentiating the analytical expression for concentration. For large uncertainties in initial conditions (as in risk assessments), the probability of each initial condition can be estimated.

8. Summary and conclusions

(1) Analytical equations for the ensemble mean instantaneous concentration within an instantaneously released dense gas cloud are valid within both the dense and neutral regimes of the cloud's lifetime. The correction term σ_m for molecular diffusion within small releases can be ignored. Other factors such as mixing height, heat transfer, and presence of aerosols are also ignored. The model also calculates cloud height, radius, acceleration, and drift.

(2) The model provides a smooth transition of all properties from the dense regime to the neutral buoyancy regime. Furthermore, there is no localized time at which transition occurs; rather, it is very gradual. The timing and conditions for transition have been of great concern for many modeling systems consisting of a separate dense gas box model and a separate Gaussian model. The difficulty of such a system can be seen in Fig. 3. Using $Ri_l = 10^5$ as an example, the dashed line to the left of the Gaussian is the dense gas model solution. The intersection of the two lines marks the point at which transition would be assumed. However, the present model (assumed to be an improvement) suggests that concentrations remain about an order of magnitude above the Gaussian and become very slowly asymptotic to it as time progresses.

(3) The normalized maximum concentration C_b/C_0 is primarily a function of two variables: t/τ and Ri_l.

(4) The calibration constants have the following values: $a_1 = 1.16$, $a_3 = 0.35$, $c_1 = 0.05$, $c_2 = 0.5$, $Ri_c = 0.1$, and $c_3 = 0.58$.

(5) The two laboratory studies allowed us to estimate the relative contributions of inherent and model uncertainties to the total variance within the ensemble mean estimate. Although the environmental conditions were quite different in each study, as was the total variance T^2, the relative contributions of I^2 and M^2 were the same, i.e., 32% and 68% respectively. The relative con-

tributions cannot be calculated so directly for field studies. However, because the model seems to behave as successfully for large scale as for small scale, we suspect that the relative contributions are similar. For model application, information on the partitioning of the variance is not required. The relatively large inherent uncertainty is possibly one important reason why simple models are often as reliable as complex models.

(6) The ratio method was used to compare modelled and measured concentrations and drift distances. The ratio statistics permit a best estimate of the mean and variance of the measured distribution. For general applications in the atmosphere, it is suggested that concentration estimates be made using the statistical results $\mathscr{R} \approx 1.0$ and $\sigma_{\mathscr{R}'}/\mathscr{R} \approx 0.6$. The drift model can use $\mathscr{R} \approx 1.0$ and $\sigma_{\mathscr{R}'}/\mathscr{R} \approx 0.15$ (TI results of Table 2). In order to calculate the probability of exceeding given concentrations, it is preferable to assume a normal distribution of logarithms of concentration ratios $\ln \mathscr{R}'$. Using eqs. (63), or the TI results of Table 1, $\langle \ln \mathscr{R}' \rangle \approx 0.0$ and $\sigma_{\ln \mathscr{R}'} \approx 0.6$ (or $\sigma_{\log \mathscr{R}'} \approx 0.3$).

Acknowledgements

I am very appreciative of several helpful comments provided by John Walmsley (Atmospheric Environment Service) and by the reviewer for this paper. These have been incorporated into the paper.

References

1 C.S. Matthias, Dispersion of a dense cylindrical cloud in calm air, J. Hazardous Materials, 24 (1990) 39–65.
2 C.J. Wheatley and D.M. Webber, Aspects of the dispersion of denser-than-air vapours relevant to gas cloud explosions, Report No. EUR 9592 EN, Commission of the European Communities, Brussels, 1984.
3 R.E. Britter, Atmospheric dispersion of dense gases, Annu. Rev. Fluid Mech., 21 (1989) 317–344.
4 R.E. Britter, A review of some mixing experiments relevant to dense gas dispersion, In: J.S. Puttock (Ed.), Stably Stratified Flow and Dense Gas Dispersion, Clarendon Press, Oxford, 1988, pp. 1–38.
5 D.M. Webber, Gravity spreading in dense gas dispersion models, In: G. Ooms and H. Tennekes (Eds.), Atmospheric Dispersion of Heavy Gases and Small Particles, Springer Verlag, Berlin, 1984, pp. 397–406.
6 J.S. Turner, Buoyancy Effects in Fluids, Cambridge University Press, London, 1973.
7 J.A. Fay, The spread of oil slicks on a calm sea, In: D.P. Hoult (Ed.), Oil on the Sea, Plenum, New York, NY, 1969, pp. 53–63.
8 S. Byggstoyl and L.R. Saetran, An integral model for gravity spreading of heavy gas clouds, Atmos. Environ. 17 (1983) 1615–1620.
9 S.R. Hanna, G.A. Briggs and R.P. Hosker, Jr. (Eds.), Handbook on Atmospheric Diffusion, NTIS Report No. DE82002045 (DOE/TIC11223), Springfield, VA, 1982.
10 J.A. Businger, Equations and concepts, In: F.T.M. Nieuwstadt and J. van Dop (Eds.), Atmospheric Turbulence and Air Pollution Modelling, D. Reidel, Dordrecht, 1982, pp. 1–36.

11 J.C. Weil, Dispersion in the convective boundary layer. In: A. Venkatram and J.C. Wyngaard (Eds.), Lectures on Air Pollution Modelling, Am. Meteorol. Soc., Boston, MA, 1988.
12 F. Pasquill and F.B. Smith, Atmospheric Diffusion, Ellis Horwood, Chichester, 1983.
13 J.A. Havens and T.O. Spicer, Development of an atmospheric dispersion model for heavier than air gas mixtures. Vol. II: Laboratory calm air heavy gas dispersion experiments, U.S. Coast Guard Report CG-D-23-85, Washington, DC, 1985.
14 J. McQuaid, Objectives and design of the Phase I heavy gas dispersion trials, J. Hazardous Materials, 11 (1985) 1–33.
15 R.G. Picknett, Field experiments on the behaviour of dense clouds: Parts 1–3, Chemical Defence Establishment contract report Ptn-IL-1154/78/1-3, prepared for: Health and Safety Executive, Red Hill, Sheffield, 1978.
16 R.N. Meroney and A. Lohmeyer, Gravity spreading and dispersion of dense gas clouds released suddenly into a turbulent boundary layer, prepared for: Gas Research Institute, Contract No. 5014-352-0203, Chicago, IL, 1982.
17 R.E. Britter and J. McQuaid, Workbook on the Dispersion of Dense Gases, HSE contract report No. 17/1988, Health and Safety Executive, Sheffield, 1988.
18 P.W.M. Brighton, Area-averaged concentrations, height scales and mass balances, J. Hazardous Materials, 11 (1985) 189–208.
19 A. Venkatram, Topics in applied dispersion modelling, In: A. Venkatram and J.C. Wyngaard (Eds.), Lectures on Air Pollution Modelling, Am. Meteorol. Soc., Boston, MA, 1988.
20 D.G. Fox, Judging air quality model performance, Bull. Am. Meteorol. Soc., 62 (1981) 599–609.
21 M.H. Dickerson and D.L. Ermak, The evaluation of emergency response trace gas and dense gas dispersion models, In: M.L. Kramer and W.M. Porch (Eds.), Meteorological Aspects of Emergency Response, Am. Meteorol. Soc., Boston, MA, 1990.